Implications of isoscalar and isovector scalar meson mixed interaction on nuclear and neutron star properties

Sunil Kumar [1,*] Mukul Kumar [1,†] Raj Kumar [1,‡] and Shashi K. Dhiman [1,2,§]

[1]*Department of Physics, Himachal Pradesh University, Shimla-171005, India*

[2]*School of Applied Sciences, Himachal Pradesh Technical University, Hamirpur-177001, India*

(Received 21 July 2023; accepted 19 October 2023; published 15 November 2023)

The properties of finite nuclei, bulk nuclear matter, and neutron stars are studied using the relativistic mean field model which includes nonlinear couplings between isoscalar and isovector mesons. The quartic interaction $\sigma^2\delta^2$ due to isoscalar and isovector scalar, σ and δ mesons, is also taken into account in addition to vector meson mixing $\omega^2\rho^2$. Several HPNL sets (named from Himachal Pradesh University Nuclear Laboratory) are generated to assess the influence of isoscalar and isovector scalar meson mixed interactions $\sigma^2\delta^2$ on the density dependence of symmetry energy and neutron star properties. These parametrizations correspond to different values of coupling constant, $\Lambda_{\sigma\delta}$ of σ-δ meson mixing and are obtained by fitting the available experimental data of ground state properties (binding energies and charge radii) for finite nuclei, infinite nuclear matter, and observed maximum mass of PSR J0740+6620 by following the χ^2 minimization procedure. Furthermore, the σ-δ mixing is found to have a large influence on the radius and tidal deformability of a canonical neutron star. These new relativistic interactions are found to be simultaneously compatible with the constraints on the equation of state of symmetric nuclear and pure neutron matter from particle flow data in heavy ion collisions, the neutron skin thickness of ^{208}Pb from PREX-II results, the mass-radius relations measured from NICER, and the limits of dimensionless tidal deformability of a canonical neutron star from binary neutron star merger GW170817 and GW190814 events.

DOI: 10.1103/PhysRevC.108.055802

I. INTRODUCTION

The astrophysical phenomena concerning compact stars as well as the finite nuclei and nuclear matter properties are determined by the nuclear equation of state (EoS) that is established by the relationship between the energy density and pressure of the system. As a result of precise observations of neutron stars, such as the Shapiro delay measurement of a binary millisecond pulsar J1614+2230 [1,2] and the radius measurement of PSR J0740+6620 from the Neutron Star Interior Composition Explorer (NICER) and from x-ray multi-mirror (XMM- Newton) data [3,4], theoretical studies have been currently performed more than ever to explain the neutron star physics through the EoS for dense nuclear matter. In addition, the direct detection of gravitational-wave (GW) signals from a binary neutron star merger, GW170817, observed by advanced LIGO and Virgo detectors have placed stringent constraints on the mass–radius relation of neutron stars [5–7]. The tidal deformability of a neutron star [8,9] has a very significant role to construct EoS of the neutron star.

The lead radius experiment (PREX-II) has recently given a model-independent extraction of neutron skin thickness of ^{208}Pb as $\Delta r_{np} = 0.283 \pm 0.071$ fm [10]. The Δr_{np} has been identified as an ideal probe on symmetry energy—a key but poorly known quantity that describes the isospin dependence of EoS of nuclear matter and plays a very important role in various concerns in atomic physics and astrophysics. Reed *et al.* [11] had proposed a large value of density dependence of symmetry energy $L = 106 \pm 37$ MeV to explain the PREX-II result and suggested a strong positive linear correlation of neutron skin thickness of the lead nucleus with the slope of symmetry energy (L) at saturation density. The value of L around the saturation density strongly affects the mass-radius relation and tidal deformability (Λ) of a neutron star. It provides a unique bridge between atomic nuclei and neutron stars. The large value of $\Delta r_{np} = 0.283 \pm 0.071$ fm suggests a very stiff EoS and large value of L around saturation density and generally gives rise to a large value of neutron star radius and the tidal deformability [11]. The upper limit on $\Lambda_{1.4} \leqslant 580$ for GW170817 requires softer EoS and hence softer symmetry energy coefficient [6]. The heaviest neutron star $2.14^{+0.10}_{-0.09} M_\odot$ of PSRJ0740+6620 [12] also limits the EoS for symmetric nuclear matter (SNM). The flow data from heavy ion collisions suggest that the EoS for SNM should be relatively softer [13].

The recent precise parity-violating electron scattering experiments on ^{208}Pb (PREX-II) [10] and ^{48}Ca (CREX) [14] provide new insights into the neutron skin thickness of nuclei. The weak charge form factors of ^{48}Ca and ^{208}Pb reported by CREX and PREX-II experiments and their measured parity-violating asymmetry have been analyzed using density functionals and reached a conclusion that it is difficult to

*sunilkumar88001@gmail.com
†mukulpathania120495@gmail.com
‡raj.phy@gmail.com
§shashi.dhiman@gmail.com

describe parity-violating asymmetry simultaneously in both nuclei [15,16]. The calcium radius experiment (CREX) has recently given a model-independent extraction of neutron skin thickness of ^{48}Ca as $\Delta r_{np} = 0.121 \pm 0.026$ fm [14] which suggests softness of density dependence of symmetry energy. It is very difficult to understand the result from the PREX-II experiment because the measured neutron skin thickness is remarkably larger than those expected theoretically. The calculations of neutron skin are generally constrained by the nuclear symmetry energy coefficient J, and its slope parameter L, near the nuclear saturation density, mainly describing the properties of isospin-asymmetric nuclear matter and heavy nuclei. A large number of theoretical nuclear studies on L via the nuclear EoS have been performed since the PREX-II experiment. Some calculations favor the small value of $L \leqslant 70$ MeV, for example, the energy density functionals or the Bayesian inference [15,17–21], whereas the others employ the larger L than 100 MeV [11,22] to account for the PREX-II results, the experimental analyses of heavy-ion collisions, and the astrophysical observations of neutron stars. However, it is still hard to determine the exact value of L [23]. In the previous works [19,20,24–26], we have developed the relativistic mean-field (RMF) models which include all possible self- and mixed-coupling terms for the σ, ω, ρ, and δ mesons up to the quartic order so that the parameters should obey the naturalness behavior as imposed by the effective field theory [27] and can simultaneously accommodate the properties of finite nuclei, bulk nuclear matter, and neutron stars within the astrophysical observations. In the present study, we construct parametrizations to assess the influence of isoscalar and isovector scalar meson mixed interactions $\sigma^2\delta^2$ on the density dependence of symmetry energy, finite nuclei, and bulk nuclear matter and neutron star properties.

The aim of the present study is to construct new effective interactions to investigate the effects of quartic interaction of a σ-δ meson on the properties of finite nuclei, bulk nuclear matter, and asymmetric dense nuclear matter within the framework of the RMF model. We generate several parameter sets by varying the coupling strength ($\Lambda_{\sigma\delta}$) of σ-δ meson mixing with the remaining ones calibrated to yield finite nuclei, bulk nuclear matter, and neutron star properties consistent with the available terrestrial experiments and astrophysical observations of neutron stars. It is necessary that the equations of state (EoSs) obtained with these new RMF effective interactions should be compatible with the constraints on EoSs of symmetric nuclear and pure neutron matter from particle flow data from heavy ion collisions, the neutron skin thickness of ^{208}Pb from PREX-II results, the mass-radius relations measured from NICER, and the limits of dimensionless tidal deformability of canonical neutron star from both binary neutron star merger events, GW170817 ($\Lambda_{1.4} = 190^{+390}_{-120}$) [6] and GW190814 ($\Lambda_{1.4} = 616^{+273}_{-158}$) [28].

The paper is organized as follows, a brief summary of the RMF model with nonlinear, self-, and cross-couplings has been provided in Sec. II. In Sec. III, we present our numerical results and detailed discussions. Finally, we summarize the results of the present work in Sec. IV.

II. THEORETICAL MODEL

The recently updated model for Lagrangian density in RMF approximation is motivated for the construction of the EoS for nuclear and neutron star matter. The effectiveLagrangian density for the RMF model generally describes the interaction of the baryons via the exchange of σ, ω, ρ, and δ mesons up to the quartic order. The Lagrangian density [20,24,26,29] of the nucleon system is given by

$$\begin{aligned}\mathcal{L} = \sum_{N=n,p} \overline{\Psi}_N \Big[& i\gamma^\mu \partial_\mu - (M_N - g_{\sigma N}\sigma - g_{\delta N}\delta.\tau_N) \\ & - \left(g_\omega \gamma^\mu \omega_\mu + \frac{1}{2} g_\rho \gamma^\mu \tau_N.\rho_\mu + e\gamma_\mu \frac{1+\tau_{3N}}{2} A_\mu \right) \Big] \Psi_N \\ & + \frac{1}{2}\left(\partial_\mu \sigma \partial^\mu \sigma - m_\sigma^2 \sigma^2\right) - \frac{\overline{\kappa}}{3!} g_{\sigma N}^3 \sigma^3 - \frac{\overline{\lambda}}{4!} g_{\sigma N}^4 \sigma^4 \\ & - \frac{1}{4}\omega_{\mu\nu}\omega^{\mu\nu} + \frac{1}{2} m_\omega^2 \omega_\mu \omega^\mu + \frac{1}{4!}\zeta g_{\omega N}^4 (\omega_\mu \omega^\mu)^2 \\ & - \frac{1}{4}\rho_{\mu\nu}\rho^{\mu\nu} + \frac{1}{2} m_\rho^2 \rho_\mu \rho^\mu + \frac{1}{2}\left(\partial_\mu \delta \partial^\mu \delta - m_\delta^2 \delta^2\right) \\ & - \frac{1}{4} F_{\mu\nu} F^{\mu\nu} + \frac{1}{2}\Lambda_{\omega\rho} g_{\omega N}^2 g_{\rho N}^2 \omega_\mu \omega^\mu \rho_\mu \rho^\mu \\ & + \Lambda_{\sigma\delta} g_{\sigma N}^2 g_{\delta N}^2 \sigma^2 \delta^2 + \sum_{\ell=e,\mu} \overline{\Psi}_\ell (i\gamma^\mu \partial_\mu - M_\ell)\Psi_\ell, \end{aligned} \tag{1}$$

where M_N is the nucleon mass, (m_σ, m_ω, m_ρ, m_δ) are the meson masses, and ($g_{\sigma N}$, $g_{\omega N}$, $g_{\rho N}$, $g_{\delta N}$) represent coupling constants for nucleons with the corresponding mesons. In addition $\overline{\kappa}$, $\overline{\lambda}$ are the self-interaction coefficients of the σ meson, and ζ represents the self-interaction coefficient of the ω meson. For cross coupling terms we have included coefficients ($\Lambda_{\omega\rho}$, $\Lambda_{\sigma\delta}$) which represent coupling between ($\omega - \rho$), ($\sigma - \delta$) mesons, respectively, in the Lagrangian density.

To obtain the equation of motion for nucleons and mesons one can solve the standard Euler-Lagrange equation of motion [24,26,29] as

$$\partial_\mu \left(\frac{\partial \mathcal{L}}{\partial(\partial_\mu \phi)} \right) - \frac{\partial \mathcal{L}}{\partial \phi} = 0. \tag{2}$$

The equation of motion for baryons, mesons, and photons can be derived from the Lagrangian density defined in Eq. (1). The equation of motion for baryons can be given as

$$\begin{aligned}\Big[& \gamma^\mu \left(i\partial_\mu - g_{\omega N}\omega_\mu - \frac{1}{2} g_{\rho N}\tau_N.\rho_\mu - e\frac{1+\tau_{3B}}{2} A_\mu \right) \\ & - (M_N - g_{\sigma N}\sigma - g_{\delta N}\delta \cdot \tau_3) \Big] \Psi_N = \epsilon_N \Psi_N. \end{aligned} \tag{3}$$

The Euler-Lagrange equations for the ground-state expectation values of the mesons fields are

$$\begin{aligned}\left(-\Delta + m_\sigma^2\right)\sigma = & \sum_N g_{\sigma N}\rho_{sN} - \frac{\overline{\kappa}}{2} g_{\sigma N}^3 \sigma^2 - \frac{\overline{\lambda}}{6} g_{\sigma N}^4 \sigma^3 \\ & + 2\Lambda_{\sigma\delta} g_{\sigma N}^2 g_{\delta N}^2 \sigma \delta^2, \end{aligned} \tag{4}$$

$$\left(-\Delta + m_\omega^2\right)\omega = \sum_N g_{\omega N}\rho_N - \frac{\zeta}{6}g_{\omega N}^4\omega^3 - \Lambda_{\omega\rho}g_{\omega N}^2 g_{\rho N}^2\omega\rho^2, \quad (5)$$

$$\left(-\Delta + m_\rho^2\right)\rho = \sum_N g_{\rho N}\tau_{3N}\rho_N - \Lambda_{\omega\rho}g_{\omega N}^2 g_{\rho N}^2\omega^2\rho, \quad (6)$$

$$\left(-\Delta + m_\delta^2\right)\delta = \sum_N g_{\delta N}\rho_{s3N} + 2\Lambda_{\sigma\delta}g_{\sigma N}^2 g_{\delta N}^2\sigma^2\delta \quad (7)$$

$$-\Delta A_0 = e\rho_p, \quad (8)$$

where the baryon vector density ρ_N, scalar density ρ_{sN}, and charge density ρ_p are, respectively,

$$\rho_N = \langle\overline{\Psi}_N\gamma^0\Psi_N\rangle = \frac{\gamma k_N^3}{6\pi^2}, \quad (9)$$

$$\rho_{sN} = \langle\overline{\Psi}_N\Psi_N\rangle = \frac{\gamma}{(2\pi)^3}\int_0^{k_N} d^3k\frac{M_N^*}{\sqrt{k^2 + M_N^{*2}}}, \quad (10)$$

$$\rho_N = \left\langle\overline{\Psi}_N\gamma^0\frac{1+\tau_{3N}}{2}\Psi_N\right\rangle \quad (11)$$

with γ the spin-isospin degeneracy. The Dirac effective mass for the neutron and proton can be written as

$$M_p^* = (M_N - g_\sigma\sigma - g_\delta\delta), \quad (12)$$

$$M_n^* = (M_N - g_\sigma\sigma + g_\delta\delta). \quad (13)$$

Following the Euler-Lagrange formalism one can readily find the expressions for energy density $\mathcal{E}$ and pressure P as a function of density from Eq. (1) [30]. From Lagrangian density one can also obtain the energy-momentum ($\mathcal{T}^{\mu\nu}$) tensor, which can be used to find pressure ($\mathcal{P}$) and energy density ($\mathcal{E}$) [31,32]:

$$\mathcal{T}^{\mu\nu} = \sum_{\phi_a}\frac{\partial\mathcal{L}}{\partial(\partial_\mu\phi_a)}\partial^\nu\phi_a - g^{\mu\nu}\mathcal{L}, \quad (14)$$

$$\mathcal{P} = \frac{1}{3}\sum_{j=1}^{3}\langle\mathcal{T}^{jj}\rangle, \quad (15)$$

$$\mathcal{E} = \langle\mathcal{T}^{00}\rangle. \quad (16)$$

III. RESULTS AND DISCUSSION

In this section, we discuss the optimization of model parameters for RMF models. The model parametrizations obtained are then used to calculate the properties of finite nuclei, bulk nuclear matter, and neutron stars.

A. Parametrizations of RMF model

In the present study, seven new relativistic interactions HPNL, HPNL0, HPNL1, HPNL2, HPNL3, HPNL4, and HPNL5 have been generated for the Lagrangian density given by Eq. (1) to investigate the effect of isoscalar and isovector scalar meson mixed interactions $\sigma^2\delta^2$ on the properties of finite nuclei and neutron star matter. Here, HPNL0, HPNL1, HPNL2, HPNL3, HPNL4, and HPNL5 parametrizations correspond to different values of the isoscalar and isovector scalar meson mixed couplings ($\Lambda_{\sigma\delta}$) of σ-δ mesons, i.e., $\Lambda_{\sigma\delta}$ = 0.00, 0.01, 0.02, 0.03, 0.04, and 0.05, respectively. For the sake of comparison, we also construct the HPNL parameter set that does not include the coupling (g_δ) of the δ meson to the nucleon and couplings ($\Lambda_{\sigma\delta}$) of σ-δ mesons. As the effect of δ meson is predominantly important at suprasaturation densities, one can *a priori* anticipate its insignificant impact in finite nuclei, which is primarily sensitive to the EoS at subsaturation densities. This is the reason why we kept fixed the $\Lambda_{\sigma\delta}$ at aforementioned values optimizing the rest of the parameters in Eq. (1). This is not far from the strategy recently used by Li *et al.* in Ref. [32]. The optimization of the parameters (p) appearing in the Lagrangian [Eq. (1)] has been performed by using the simulated annealing method (SAM) [33,34] by following χ^2 minimization procedure which is given as

$$\chi^2(\mathbf{p}) = \frac{1}{N_d - N_p}\sum_{i=1}^{N_d}\left(\frac{O_i^{\rm exp} - O_i^{th}}{\sigma_i}\right)^2, \quad (17)$$

where N_d is the number of experimental data points and N_p is the number of fitted parameters. The σ_i denotes adopted errors [20,25,35] and $O_i^{\rm exp}$ and O_i^{th} are the experimental and the corresponding theoretical values, respectively, for a given observable. The model optimization in the HPNL family is performed so as to fit the experimental data [36] on binding energies (BE) and charge rms radii (r_{ch}) [37] of some spherical nuclei ^{16,24}O, ^{40,48}Ca, ^{56,68,78}Ni, ^{88}Sr, ^{90}Zr, ^{100,116,132}Sn, ^{144}Sm, and ^{208}Pb. For the open shell nuclei, the pairing has been included using Bardeen-Cooper-Schrieffer formalism with constant pairing gaps [20,38,39] that are taken from the nucleon separation energies of neighboring nuclei [36]. Neutron and proton pairing gaps are evaluated by using the fourth-order finite difference mass formula (five-point difference) [40]. The pairing correlation energies for a fixed gap Δ is calculated by using the paring window of $2\hbar\omega$, where $\hbar\omega = 45A^{-1/3}$–$25A^{-2/3}$ MeV [21]. We also incorporated the recently measured neutron skin thickness of ^{208}Pb ($\Delta r_{np} = 0.283 \pm 0.071$ fm) using the parity-violating electron scattering experiment [10] in our fit data to constrain the density dependence of symmetry energy. In addition, we have also included the observed maximum neutron star mass $M = 2.08 \pm 0.07$ $M_\odot$ for pulsar PSR J0740+6620 determined by relativistic Shapiro time delay [41] in our fitting protocol. We have incorporated the maximum mass of the neutron star in our fitting protocol to constrain the high density behavior of the equation of state. As reported in Refs. [21,29,42,43], the ω meson self-interaction term ζ plays an important role in determining the soft and stiff behavior of EoS at high densities. The neutron-star mass decreases with the increase in value of the coupling term ζ [21,29,42,43]. So, by including the maximum mass of the neutron star in the fitting protocol, we can constrain the coupling term ζ and hence soft and stiff behavior of EoS at high densities.

The model parameters for HPNL's parametrizations are searched by fitting the available experimental data on finite nuclei, bulk nuclear matter, and observed maximum neutron star mass of PSR J0740+6620 [41] by following the χ^2 minimization procedure based on Eq. (17). The HPNL's parametrizations obtained in the present work give an equally

TABLE I. Model parameters for various HPNL's models of RMF Lagrangian given in Eq. (1). The parameters $\overline{\kappa}$ in fm^{-1}. The values of $\overline{\kappa}$ and $\overline{\lambda}$ are expressed in ($\times 10^{-2}$). The mass m_σ is in units of MeV. The mass for nucleon, ω, ρ, and δ meson is taken as $M_N = 939$ MeV, $m_\omega = 782.5$ MeV, $m_\rho = 770$ MeV, and $m_\delta = 983$ MeV.

Models	g_σ	g_ω	g_ρ	g_δ	$\overline{\kappa}$	$\overline{\lambda}$	$\Lambda_{\omega\rho}$	ζ	$\Lambda_{\sigma\delta}$	m_σ
HPNL	10.35592	13.38333	10.00201	0.00000	1.73624	−0.29854	0.02174	0.02422	0.00000	498.451
HPNL0	10.44500	13.44016	10.28253	1.20129	1.64916	−0.17551	0.02756	0.02466	0.00000	501.825
HPNL1	10.20379	13.01953	11.23260	2.32189	1.90575	−0.60060	0.03375	0.01976	0.01000	501.459
HPNL2	9.99613	12.59637	11.57539	2.67798	2.09276	−0.85452	0.03417	0.01621	0.02000	503.914
HPNL3	9.97109	12.68522	11.57440	2.63218	2.05093	−0.79781	0.03819	0.01783	0.03000	500.164
HPNL4	10.11818	12.81430	12.32052	2.29541	1.89353	−0.45684	0.04527	0.02201	0.04000	504.565
HPNL5	10.17421	13.02147	12.62197	2.98371	1.76088	−0.15718	0.03799	0.02520	0.05000	500.972

good fit to the properties of finite nuclei, bulk nuclear matter, and astrophysical observables. The value of χ^2 obtained after optimization of the model parameters by following Eq. (17) in a minimization procedure comes out as 1.05, 1.07, 1.10, 1.25, 1.55, 1.89, and 1.99 for HPNL, HPNL0, HPNL1, HPNL2, HPNL3, HPNL4, and HPNL5 parameter sets, respectively. In Table I we display optimum values of the model parameters for all seven HPNL's parameter sets. It can be seen that the parameter g_ρ increases with the increase in the value of $\Lambda_{\sigma\delta}$. A larger value of g_ρ is required in the presence of the $\Lambda_{\sigma\delta}$-meson mixed interactions to fit the properties of finite nuclei. As the contribution of the mixed couplings $\Lambda_{\sigma\delta}$ of σ-δ mesons is attractive, increased binding due to this coupling has to be compensated by the higher value of the repulsion by the g_ρ field. The parameter g_ρ has its lowest value for HPNL parametrization ($g_\delta = 0.00$, $\Lambda_{\sigma\delta} = 0.00$). For any finite value of δ coupling ($g_\delta > 0$), i.e., for HPNL0, HPNL1, HPNL2, HPNL3, HPNL4, and HPNL5 parametrizations, the strength of ρ-meson coupling to the nucleon (g_ρ) increases gradually.

B. Finite nuclei and infinite nuclear matter

The newly generated parametrizations HPNL's give a good fit to the properties of finite nuclei. The binding energies (B/A) and charge radii (r_{ch}) of several closed/open-shell nuclei obtained using HPNL's parametrizations are summarized in Table II and in harmony with the available experimental data [36,49]. In addition, we have also given the root relative squared errors (RRSEs),

$$\Delta_{RRSE} = \sqrt{\frac{1}{n}\sum_{i=1}^{n}\left(\frac{X_i^{\rm exp} - X_i^{\rm calcu}}{X_i^{\rm exp}}\right)^2}, \qquad (18)$$

for $X = B/A$ and r_{ch} in the last column of Table II. It is observed that the HPNL family can reproduce the properties of finite nuclei very well. The neutron skin thickness for ^{208}Pb comes out to be 0.259, 0.245, 0.226, 0.220, 0.213, 0.207, and 0.206 fm for HPNL parametrizations, respectively, and is in close proximity with the limits put by PREX-II results [10,15]. The values of the neutron skin thickness of $\Delta r_{np}(^{48}\text{Ca})$ predicted for these parametrizations 0.220, 0.213, 0.204, 0.201, 0.197, 0.193, 0.194 fm, respectively, are overestimated with the CREX results reported in Ref. [14]. The theoretical results for $\Delta r_{np}(^{48}\text{Ca})$ obtained for HPNL1, HPNL2, HPNL3, HPNL4, and HPNL5 parametrizations are well consistent with the experimental data: the electrical dipole polarizability of ^{48}Ca RCNP; $(\Delta r_{np}) = 0.14$–0.20 fm [50]. Therefore it is very hard to satisfy the PREX-II and CREX results simultaneously even if we include the δ-N and σ-δ mixing interactions in the RMF model.

In Table III, we present our results for the several bulk properties of symmetric nuclear matter (SNM) at the saturation density. The properties such as binding energy per nucleon (E/A), incompressibility (K), symmetry energy coefficient (J), density dependence of symmetry energy (L), and the ratio of effective mass to the mass of nucleon (M_N^*/M_N). The Q_0 represents the third order of incompressibility coefficient of SNM around saturation density ρ_0. $K_{\rm sym}$ and $Q_{\rm sym}$ are the curvature parameter of symmetry energy and third order coefficient of symmetry energy around ρ_0, respectively. The $K_{\rm sat,2}$ (K_τ) characterize the isospin dependence of incompressibility of asymmetric nuclear matter and K_N reflects the neutron matter incompressibility. The bulk properties are given by the coefficients in the power series expansion of asymmetric nuclear EoS around ρ_0 [51]. The $K_{\rm sat,2}$ (K_τ) and K_N are expressed as $K_{\rm sat,2} = K_{\rm sym} - 6L - \frac{Q_0 L}{K}$ and $K_N = K_{\rm sym} + K$ [52,53]. These properties play a very important role in constructing the EoS for dense nuclear matter. These bulk nuclear matter parameters characterize the EoS of asymmetric nuclear matter and its density dependence at normal nuclear density ρ_0. They provide reliable information concerning the isospin dependence of saturation properties of asymmetric nuclear matter as well as its properties at both low and high densities. In Table III, E/A is more or less the same for all HPNL parametrizations. The value of nuclear incompressibility K lies in the range 224.09–234.04 MeV which is consistent with the value of $K = 240 \pm 20$ MeV determined from the isoscalar giant monopole resonance (ISGMR) for ^{90}Zr and ^{208}Pb nuclei [54,55]. It can be observed from Tables I and III that the value of the slope of symmetry energy L is strongly correlated with coupling $\Lambda_{\sigma\delta}$ of σ-δ mesons. HPNL interactions cover a wide range of couplings $\Lambda_{\sigma\delta}$ of σ-δ mesons mixed interactions. As we move from the HPNL0 model ($\Lambda_{\sigma\delta} = 0.0$) to the HPNL5 model ($\Lambda_{\sigma\delta} = 0.05$), the value of L decreases from 78.38 MeV to 52.29 MeV. The values of J and L obtained by HPNL, HPNL0 parametrizations are consistent with the values $J = 38.1 \pm 4.7$ MeV and $L = 106 \pm 37$ MeV as inferred by Reed *et al.* [11]. The values of J and L at saturation density calculated for HPNL1,

TABLE II. Theoretical calculations of ground state properties, binding energy (B/A), and charge radii r_{ch} of closed/open-shell nuclei for various HPNL models. Experimental data for binding energy per nucleon and charge radius are taken from [36,37,44].

	B/A (MeV)														
Models	^{16}O	^{24}O	^{40}Ca	^{48}Ca	^{56}Ni	^{68}Ni	^{78}Ni	^{88}Sr	^{90}Zr	^{100}Sn	^{116}Sn	^{132}Sn	^{144}Sm	^{208}Pb	$\Delta_{RRSE}(\%)$
HPNL	−8.003	−7.103	−8.585	−8.647	−8.605	−8.712	−8.217	−8.726	−8.708	−8.284	−8.516	−8.352	−8.321	−7.874	0.358
HPNL0	−8.034	−7.114	−8.587	−8.654	−8.607	−8.710	−8.225	−8.722	−8.701	−8.275	−8.508	−8.351	−8.313	−7.867	0.417
HPNL1	−8.044	−7.080	−8.599	−8.647	−8.581	−8.712	−8.216	−8.723	−8.703	−8.262	−8.514	−8.353	−8.317	−7.875	0.409
HPNL2	−8.092	−7.055	−8.630	−8.651	−8.572	−8.715	−8.193	−8.728	−8.709	−8.258	−8.518	−8.338	−8.319	−7.863	0.567
HPNL3	−7.999	−7.017	−8.582	−8.622	−8.545	−8.700	−8.196	−8.715	−8.696	−8.244	−8.512	−8.350	−8.315	−7.879	0.422
HPNL4	−8.043	−7.024	−8.594	−8.640	−8.576	−8.706	−8.205	−8.719	−8.698	−8.252	−8.508	−8.350	−8.311	−7.869	0.392
HPNL5	−8.067	−6.999	−8.630	−8.650	−8.593	−8.720	−8.183	−8.743	−8.727	−8.286	−8.538	−8.347	−8.343	−7.886	0.545
Experiments	−7.976	−7.040	−8.551	−8.666	−8.643	−8.682	−8.238	−8.732	−8.709	−8.251	−8.523	−8.350	−8.304	−7.867	–
	r_{ch} (fm)														
HPNL	2.711	2.73	3.454	3.461	3.712	3.857	3.942	4.218	4.273	4.512	4.606	4.711	4.954	5.520	0.308
HPNL0	2.710	2.735	3.458	3.469	3.720	3.867	3.953	4.229	4.284	4.523	4.619	4.725	4.968	5.535	0.321
HPNL1	2.712	2.741	3.455	3.470	3.721	3.868	3.953	4.227	4.281	4.521	4.616	4.721	4.963	5.528	0.311
HPNL2	2.702	2.737	3.443	3.463	3.718	3.861	3.946	4.217	4.270	4.513	4.605	4.710	4.950	5.513	0.327
HPNL3	2.701	2.732	3.436	3.453	3.704	3.849	3.932	4.203	4.257	4.497	4.589	4.692	4.932	5.492	0.517
HPNL4	2.689	2.725	3.428	3.447	3.693	3.844	3.928	4.198	4.252	4.487	4.585	4.689	4.928	5.489	0.664
HPNL5	2.707	2.747	3.452	3.475	3.729	3.875	3.961	4.232	4.285	4.527	4.621	4.728	4.967	5.534	0.386
Experiments	2.699	–	3.478	3.477	3.723	–	–	4.224	4.269	–	4.625	4.709	4.952	5.501	–

HPNL2, HPNL3, HPNL4, and HPNL5 parametrizations are consistent with the constraints from the observational analysis $J = 31.61 \pm 2.66$ and $L = 58.9 \pm 16$ MeV [56] and also satisfies the recently reported limit $L = 54 \pm 8$ MeV [15] and $L = 15.3^{+46.8}_{-41.5}$ [57]. The value of the curvature of symmetry energy $K_{\rm sym}$ for HPNL's parameter sets also satisfies the theoretical analyses based on neutron star observables, $K_{\rm sym} \approx -107 \pm 88$ MeV [47] and empirical limit discussed in [58]. The value of neutron matter incompressibility, K_N, is also in good agreement with that predicted by chiral effective field theory, $K_N = 152.2 \pm 38.2$ MeV [53]. Furthermore, the asymmetry term of nuclear incompressibility, K_τ, for the HPNL and HPNL0 parameter sets satisfy the experimental constraints from isoscalar giant monopole resonance in the Sn and Cd isotopes, $K_\tau = -550 \pm 100$ MeV [59] and $K_\tau = -555 \pm 75$ MeV [60].

In Figs. 1 and 2, we plot the EoSs, i.e., pressure as a function of baryon density scaled to saturation density ($\frac{\rho}{\rho_0}$) for SNM and pure neutron matter (PNM) using HPNL parametrizations. We also show (shaded regions) the EoSs extracted from the analysis of particle flow data in heavy ion collisions [13] and experimental data taken from Ref. [45]. It is evident from Figs. 1 and 2 that the EoSs for SNM and PNM obtained for HPNL parametrizations lie in the upper portion of the allowed region with the EoS extracted from the analysis of the particle flow in heavy ion collision [13] and from Ref. [45]. The EoS calculated for HPNL5 parametrization is the softest amongst all EoSs and it might be due to the relatively somewhat higher value of coupling $\Lambda_{\sigma\delta}$ for this parameter set. In Fig. 3, we plot the symmetry energy as a function of baryon density for various HPNL parametrizations. It is evident from the figure that the value of symmetry energy coefficient (J) increases with baryon density for various models considered in the present work. It can be noticed from the figure that in the high-density regime, the curve of J becomes softer as we move from HPNL0 to HPNL5 interactions, i.e., the value

TABLE III. Properties of symmetric nuclear matter at saturation density (ρ_0). E/A denotes the binding energy per nucleon. The bulk properties are given by the coefficients in the power series expansion of asymmetric nuclear EoS around saturation density, ρ_0 [51]. The K_τ and K_N are expressed as $\mathrm{K}_{\mathrm{sat},2}(K_\tau) = K_{\rm sym} - 6L - \frac{Q_0 L}{K}$ and $K_N = K_{\rm sym} + K$ [52,53]. All nuclear parameters except ρ_0 and M^*_N/M_N are in units of MeV. The ρ_0 is in fm^{-3}.

Models	ρ_0	M^*_N/M_N	E/A	K	Q_0	J	L	$K_{\rm sym}$	$Q_{\rm sym}$	$K_{\rm sat,2}$	K_N
HPNL	0.149	0.600	−16.17	224.09	−201.80	35.90	86.71	−66.38	310.12	−508.55	157.71
HPNL0	0.148	0.603	−16.10	227.38	−219.99	34.63	78.38	−69.63	489.01	−464.08	157.75
HPNL1	0.149	0.611	−16.13	226.95	−251.93	33.57	67.02	−71.08	893.24	−398.80	155.87
HPNL2	0.150	0.624	−16.15	234.04	−293.58	33.66	63.03	−89.01	1084.97	−388.12	145.02
HPNL3	0.152	0.616	−16.23	232.03	−263.54	33.13	60.22	−74.03	1121.46	−366.95	158.01
HPNL4	0.152	0.615	−16.19	232.74	−283.04	33.76	55.44	−62.57	1153.09	−327.79	170.17
HPNL5	0.148	0.618	−16.18	230.32	−328.05	33.04	52.29	−84.22	1186.42	−323.48	146.10

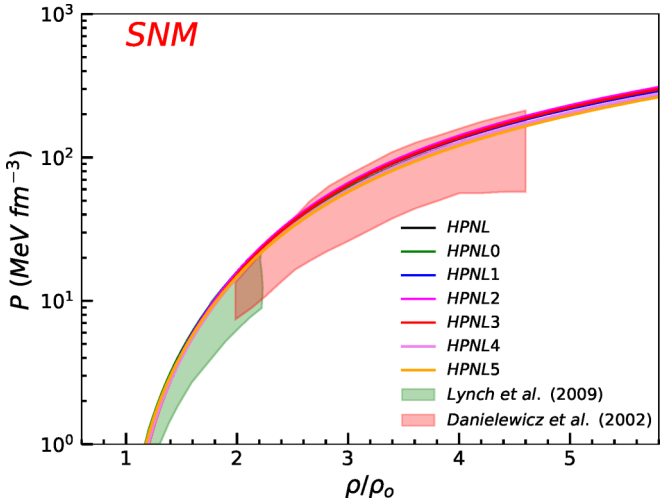

FIG. 1. Variation of pressure as a function of baryon density for symmetric nuclear matter (SNM) computed with HPNL's parametrizations. The shaded region represents the experimental data taken from Refs. [13,45].

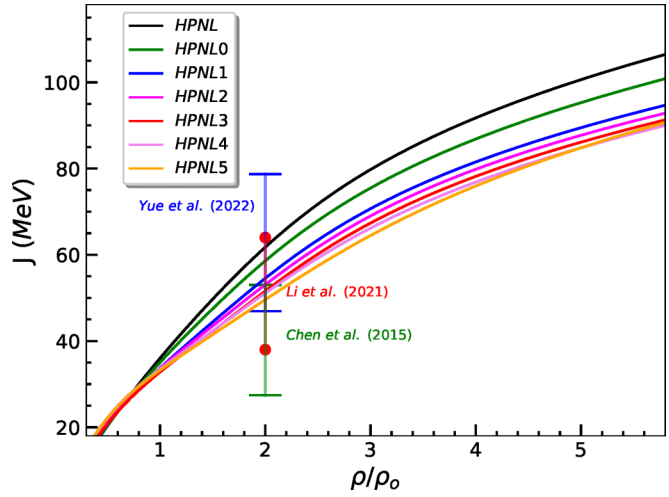

FIG. 3. Symmetry energy coefficient (J) as a function of baryon density scaled to saturation density for various HPNL parametrizations. The constraints on the magnitude of the symmetry energy coefficient at $J(2\rho_0)$: $J(2\rho_0) = 62.8 \pm 15.9$ MeV [46], $J(2\rho_0) = 51 \pm 13$ MeV from nine analyses of neutron star observables since GW170817 [47] and J($2\rho_0$) $= 40.2 \pm 12.8$ MeV based on microscopic calculations with various energy density functionals [48] are also shown.

of J is strongly correlated to mixed interaction $\Lambda_{\sigma\delta}$ of σ-δ mesons. The value of J obtained for HPNL, HPNL0, HPNL1, HPNL2 parametrizations is 61.46, 58.03, 54.28, 53.06 MeV, respectively, and satisfies the constraints on the magnitude of symmetry energy coefficient at $J(2\rho_0)$: $J(2\rho_0) = 62.8 \pm 15.9$ MeV [46], $J(2\rho_0) = 51 \pm 13$ MeV from nine new analyses of neutron star observables since GW170817 [47]. The value of J obtained for HPNL3, HPNL4, and HPNL5 parametrizations is 52.08, 51.25, and 49.16 MeV, respectively, and is well consistent with $J(2\rho_0) = 40.2 \pm 12.8$ MeV based on microscopic calculations with various energy density functionals [48]. Amongst HPNL parametrizations, the value of J is found to be stiffest for HPNL and softest for HPNL5 models in a higher density regime. This might be due to the larger value of coupling $\Lambda_{\sigma\delta}$ in the case of the HPNL5 model as this coupling term is found to play an important role in constraining the symmetry energy and its density dependence.

In Fig. 4 we depict the density dependence of symmetry energy (L) as a function of baryon density for HPNL parametrizations. The value of the slope of symmetry energy L is strongly correlated with coupling $\Lambda_{\sigma\delta}$ of σ-δ mesons. The HPNL0–HPNL5 interactions cover a wide range of couplings $\Lambda_{\sigma\delta}$ of σ-δ mesons mixed interactions. It can be seen from the figure that in low- or medium-density regimes the behavior of HPNL5 is softest (low value of L at a given baryon

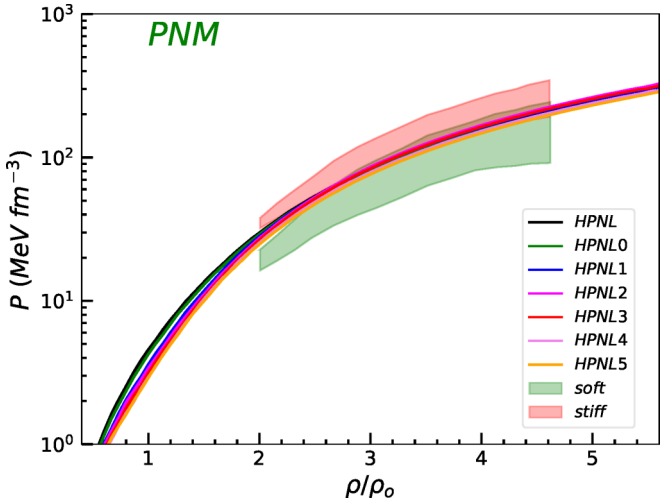

FIG. 2. Variation of pressure as a function of baryon density for pure neutron matter (PNM) computed with HPNL's parametrizations. The shaded region represents the experimental data taken from Ref. [13].

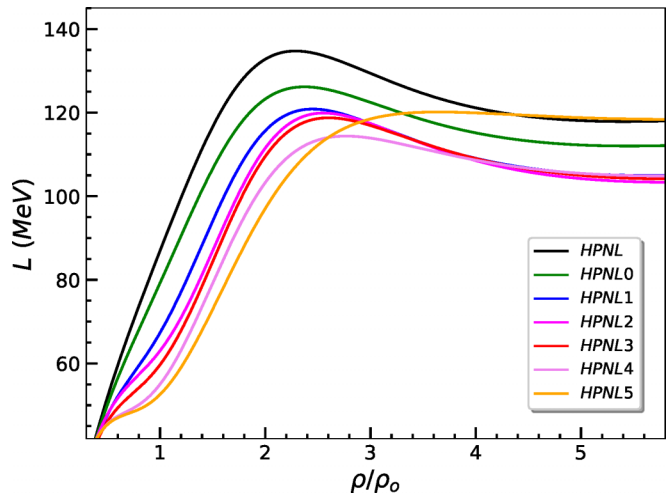

FIG. 4. Variation of density dependence of symmetry energy (L) as a function of baryon density scaled to saturation density for various HPNL parametrizations considered in the present work.

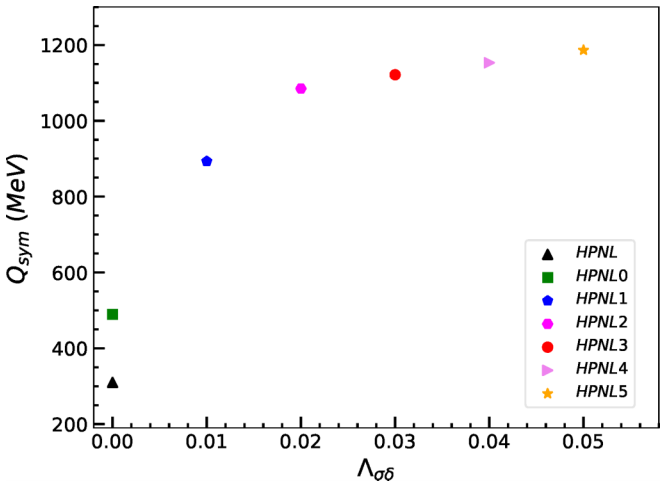

FIG. 5. Variation of third order coefficient of symmetry energy, $Q_{\rm sym}$, with coupling parameters $\Lambda_{\sigma\delta}$.

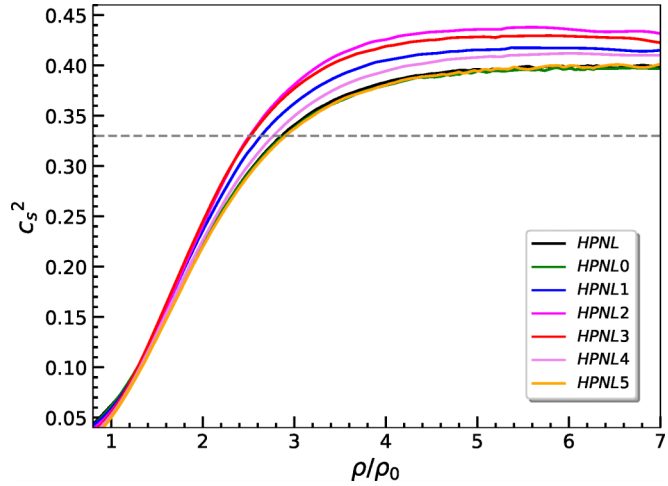

FIG. 6. Speed of sound squared as a function of scaled baryon density ρ/ρ_0 in units of speed of light squared. The horizontal dashed line represents the conformal limit given by $c_s^2 = 1/3$ [61].

density) amongst all parametrizations and changes to stiffest in high-density regimes. This may be attributed to the large value of coupling parameter $\Lambda_{\sigma\delta}$ for the HPNL5 parameter set. The large value of coupling parameter $\Lambda_{\sigma\delta}$ is responsible for changing the behavior of L from soft in low and medium density regimes to stiff in high-density regime. The stiffness of L for HPNL0 parameter sets may also be due to not including the coupling parameter $\Lambda_{\sigma\delta}$ whereas in the case of the HPNL parameter set, the stiffness of L might be due to not including δ-N coupling parameter g_δ, which is responsible for softening of EoS in the low to medium density regime [20] and noninclusion of mixed-coupling $\Lambda_{\sigma\delta}$.

In Fig. 5 the dependence of third order coefficient of symmetry energy, $Q_{\rm sym}$, on mixed interaction coupling parameter $\Lambda_{\sigma\delta}$ of σ-δ mesons is depicted. The value of $Q_{\rm sym}$ shows strong dependence on $\Lambda_{\sigma\delta}$ and increases with $\Lambda_{\sigma\delta}$. The value of $Q_{\rm sym}$ increases from 489.01 MeV to 1186.42 MeV as we proceed from HPNL0 ($\Lambda_{\sigma\delta} = 0.00$) to HPNL5 ($\Lambda_{\sigma\delta} = 0.05$) interactions. The value of $Q_{\rm sym}$ calculated for the HPNL parameter set that does not include the coupling g_δ and $\Lambda_{\sigma\delta}$ comes out to be 310.12 MeV.

C. Neutron star properties

In this subsection the model parametrizations obtained are used to calculate the properties of neutron stars like maximum mass, radius, and tidal deformability.

In Fig. 6 we display the speed of sound squared c_s^2 in neutron star matter as a function of scaled baryon density ρ/ρ_0, where the condition of charge neutrality and β equilibrium under weak processes are established. The horizontal dashed line represents the conformal limit given by $c_s^2 = 1/3$ [61]. As discussed by Alford *et al.* [61], the c_s^2 for all HPNL parametrizations lies above the conformal limit $c_s^2 = 1/3$ at high densities. The c_s^2 rises slowly with density and stays almost constant at high densities. The rapid growth in c_s^2 for HPNL parametrizations occurs around 2.5 ρ_0, where the EoS of dense nuclear matter changes due to δ-Nf and σ-δ mesons mixing.

In order to discuss the properties of neutron stars, the low-density EoS which covers the crust region of a neutron star must be taken into consideration. The radius of canonical neutron stars is found to be more sensitive to the EoS of the crust region than those of maximum mass configurations. In the present work, for the low-density region (crust), we employed Baym-Pethick-Sutherland (BPS) EoS [62] matching it to the model EoS. The mass and radius of a neutron star are obtained by solving the Tolman-Oppenheimer-Volkoff (TOV) equations [63,64] given as

$$\frac{dP(r)}{dr} = -\frac{\{\epsilon(r) + P(r)\}\{4\pi r^3 P(r) + m(r)\}}{r^2(1 - 2m(r)/r)}, \tag{19}$$

$$\frac{dm}{dr} = 4\pi r^2 \epsilon(r), \tag{20}$$

$$m(r) = 4\pi \int_0^r dr r^2 \epsilon(r), \tag{21}$$

where $P(r)$ is the pressure at radial distance r and $m(r)$ is the mass of neutron stars enclosed in the sphere of radius r. In Fig. 7, we present the results for the gravitational mass of static neutron stars and their radius for various HPNL parametrizations considered in the present work. It is observed that the maximum gravitational mass of the nonrotating neutron star for HPNL parameter sets lies in the range 2.01–2.12 $M_\odot$ which is in good agreement with the mass constraints (1.97 ± 0.04 $M_\odot$, 2.01 ± 0.04 $M_\odot$, $2.072^{+0.067}_{0.066} M_\odot$) from GW170817 event, pulsars PSR J1614+2230, PSR J0348+0432, PSR J0030+0451, and PSR J0740+6620 [1,3,4,65–68]. The radius of canonical mass ($R_{1.4}$) including BPS crust [62] for the low-density region for HPNL parametrizations lies in the range 12.75 Km–13.40 Km, which satisfies the radius constraints from NICER on $R_{1.4}$. The neutron star mass radius computed by using HPNL parametrizations are in good agreement with the NICER measurements [3,4] as shown by shaded regions labeled with NICER. The radius $R_{1.4}$ corresponding to 1.4 $M_\odot$ neutron star is also well consistent with the inferences on the

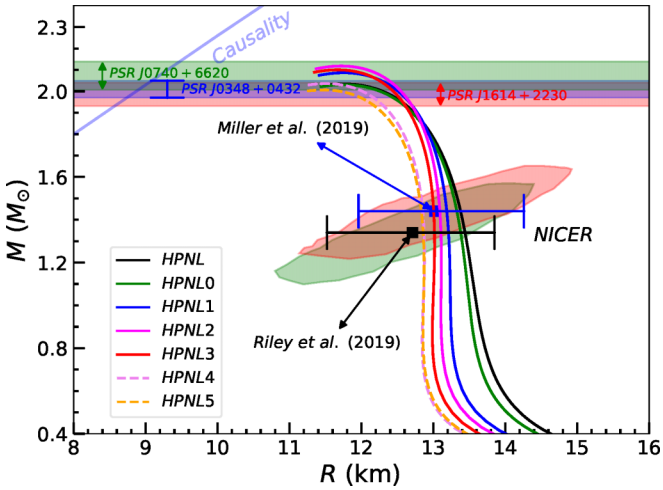

FIG. 7. Mass radius relationship of neutron star for various HPNL parametrizations. The shaded regions labeled with NICER representing the mass-radius constraints from NICER observations [3,4] are also shown.

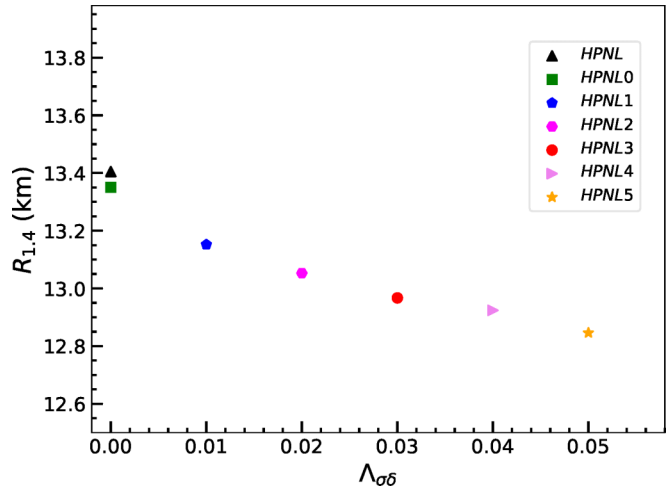

FIG. 8. Plot representing the dependence of radius $R_{1.4}$ on coupling $\Lambda_{\sigma\delta}$.

radius constraints from NICER [67–69]. It can be observed from Table IV that the radius $R_{1.4}$ has a strong dependence on mixed interaction coupling $\Lambda_{\sigma\delta}$ of σ-δ mesons. The value of radius $R_{1.4}$ decreases from 13.35 Km to 12.75 Km when we proceed from HPNL0 ($\Lambda_{\sigma\delta} = 0.00$) to HPNL5 ($\Lambda_{\sigma\delta} = 0.05$) parametrization. The value of $R_{1.4}$ is consistent with the softness and stiffness behavior of the symmetry energy coefficient. The decrease in the radius might be due to the fact the larger value of isoscalar and isovector scalar meson mixed interaction $\Lambda_{\sigma\delta}$ makes the EoSs somewhat softer in low to medium density regime.

In Fig. 8 we display a plot of radius $R_{1.4}$ and isoscalar and isovector scalar meson mixed interaction coupling $\Lambda_{\sigma\delta}$. It can be noticed from the figure that $R_{1.4}$ is strongly correlated with $\Lambda_{\sigma\delta}$. A larger value of $\Lambda_{\sigma\delta}$ might be responsible for the decrease in $R_{1.4}$ as we move from HPNL0 to HPNL5 parametrization as the slope of the symmetry energy coefficient and EoSs in the low- to medium-density regime becomes somewhat softer with the increase in coupling $\Lambda_{\sigma\delta}$. For the sake of simplicity, we have also shown the result for the HPNL model which does not include g_δ and $\Lambda_{\sigma\delta}$ coupling parameters. In Fig. 9 we show the correlations between Δr_{np} and $R_{1.4}$. The symbols (colored) in the figure express the calculated value of Δr_{np} for ^{208}Pb and ^{48}Ca. The solid line (red) is the fitting function of $\Delta r_{np}/\text{fm} = 1.0 \times 10^{-4}(R_{1.4}/\text{km})^{2.96}$ for ^{208}Pb and the solid line (blue) represents the fit $\Delta r_{np}/\text{fm} = 1.85 \times 10^{-7}(R_{1.4}/\text{km})^{5.45}$ for ^{48}Ca. In general, the larger value of $R_{1.4}$ provides the thicker neutron skin (Δr_{np}) of ^{208}Pb in the usual RMF models. Also reported by Reed *et al.*, in Ref. [11], that to satisfy the PREX-II result, L should be larger, i.e., $L = 106 \pm 37$ MeV as inferred. Meanwhile, the HPNL interactions can support the PREX-II data with the smaller value of L due to the σ-δ mesons mixed interaction coupling $\Lambda_{\sigma\delta}$. In addition, the HPNL1 to HPNL5 parametrizations also fulfill the experimental result of Δr_{np}, implied by the determination of electric dipole strength distribution in ^{48}Ca at RCNP [50]. However, it is difficult to explain the latest data reported by the CREX collaboration [14]. From this fact, we may infer that the results of the PREX-II and CREX experiments seem to be incompatible with the present calculations. The tidal deformability rendered by the companion stars on each other in a binary system can provide significant information on the EoS of neutron stars [8,9]. The tidal influences of its companion in the binary neutron star (BNS) system will deform neutron

TABLE IV. Properties of the neutron star at canonical and maximum mass for various HPNL parameter sets. The $M_{\text{max}}(M_\odot)$ and R_{max} denote the maximum gravitational mass and radius corresponding to the maximum mass of the nonrotating compact stars, respectively. The values for $R_{1.4}$ and $\Lambda_{1.4}$ and $\rho_{1.4}$ denote radius and dimensionless tidal deformability and central density at 1.4 $M_\odot$.

Models	$R_{1.4}$ (km)	$\rho_{1.4}$ (fm^{-3})	$\Lambda_{1.4}$	M_{max} ($M_\odot$)	R_{max} (km)
HPNL	13.40	0.386	671.51	2.03	11.76
HPNL0	13.35	0.387	663.67	2.03	11.75
HPNL1	13.15	0.383	641.20	2.09	11.83
HPNL2	13.05	0.385	615.96	2.12	11.78
HPNL3	12.93	0.390	596.92	2.10	11.75
HPNL4	12.80	0.405	557.14	2.04	11.50
HPNL5	12.75	0.411	548.01	2.01	11.46

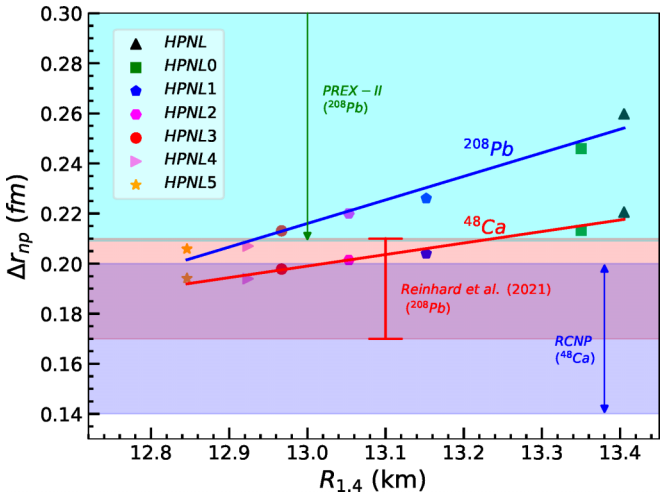

FIG. 9. Correlation between neutron skin thickness Δr_{np} and radius $R_{1.4}$. The shaded regions depict the neutron skin thickness of ^{208}Pb Δr_{np}=0.283 ± 0.071 fm from PREX-II [10], $\Delta r_{np} = 0.19 \pm 0.02$ fm) from Reinhard *et al.* [15] and Δr_{np} for ^{48}Ca ($\Delta r_{np} = 0.14$–0.20 fm) at RCNP [50].

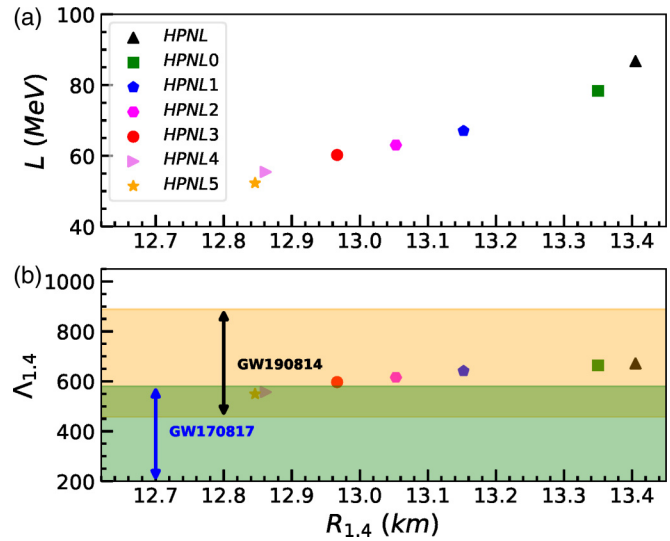

FIG. 10. (a) Correlations between the slope of symmetry energy L and radius $R_{1.4}$. (b) Correlation between $\Lambda_{1.4}$ and $R_{1.4}$. The constraints on $\Lambda_{1.4}$ from GW170817($\Lambda_{1.4} = 190^{+390}_{-120}$) [6] and GW190814 ($\Lambda_{1.4} = 616^{+273}_{-158}$) [28] are also displayed.

stars in the binary system and the resulting change in the gravitational potential modifies the BNS orbital motion and its corresponding gravitational wave (GW) signal. This effect on GW phasing can be parametrized by the dimensionless tidal deformability parameter, $\Lambda_i = \lambda_i/M_i^5$, i = 1, 2. For each neutron star, its quadrupole moment $\mathcal{Q}_{j,k}$ must be related to the tidal field $\mathcal{E}_{j,k}$ caused by its companion as $\mathcal{Q}_{j,k} = -\lambda\mathcal{E}_{j,k}$, where j and k are spatial tensor indices. The dimensionless tidal deformability parameter Λ of a static, spherically symmetric compact star depends on the neutron star compactness parameter C and a dimensionless quadrupole Love number k_2 as $\Lambda = (2k_2/3)C^{-5}$. The Λ critically parametrizes the deformation of neutron stars under the given tidal field, therefore it should depend on the EoS of nuclear dense matter. To measure the Love number k_2 along with the evaluation of the TOV equations we have to compute $y_2 = y(R)$ with initial boundary condition $y(0) = 2$ from the first-order differential equation [8,9,70,71] simultaneously,

$$y' = \frac{1}{r}[-r^2Q - ye^{\lambda}\{1 + 4\pi Gr^2(P - \mathcal{E})\} - y^2], \qquad (22)$$

where $Q \equiv 4\pi Ge^{\lambda}(5\mathcal{E} + 9P + \frac{\mathcal{E}+P}{c_s^2}) - 6\frac{e^{\lambda}}{r^2} - \nu'^2$ and $e^{\lambda} \equiv (1 - \frac{2Gm}{r})^{-1}$ and $\nu' \equiv 2Ge^{\lambda}(\frac{m+4\pi Pr^3}{r^2})$. First, we get the solutions of Eq. (22) with boundary condition, $y_2 = y(R)$, then the electric tidal Love number k_2 is calculated from the expression as

$$\begin{aligned} k_2 = \frac{8}{5}C^5(1-2C)^2[2C(y_2-1) - y_2 + 2]\Big\{2C(4(y_2+1)C^4 \\ + (6y_2 - 4)C^3 + (26 - 22y_2)C^2 \\ + 3(5y_2 - 8)C - 3y_2 + 6) - 3(1-2C)^2(2C(y_2 - 1) \\ - y_2 + 2)\ln\left(\frac{1}{1-2C}\right)\Big\}^{-1}. \end{aligned} \qquad (23)$$

In the upper panel of Fig. 10, we present the correlation between the slope of symmetry energy L and radius $R_{1.4}$. It can be observed that L is strongly intercorrelated with $R_{1.4}$. It can be inferred that a smaller value of $R_{1.4}$ favors a small value of L which in turn demands a larger coupling of $\Lambda_{\sigma\delta}$. Thus radius $R_{1.4}$ depends upon L via σ-δ meson mixing coupling $\Lambda_{\sigma\delta}$. The lower panel of Fig. 10 shows the results of dimensionless tidal deformability $\Lambda_{1.4}$ as a function of $R_{1.4}$ for the neutron star for HPNL parametrizations. It is noteworthy that the value of $\Lambda_{1.4}$ obtained for canonical mass with HPNL4 and HPNL5 parameter sets is 557.14 and 548.01 which satisfies the constraints on $\Lambda_{1.4}$ from GW170817 ($\Lambda_{1.4} = 190^{+390}_{-120}$) ($\Lambda_{1.4} \leqslant 580$ within 1σ uncertainty) [6] for the EoS of dense nuclear matter. The $\Lambda_{1.4}$ obtained for canonical mass with HPNL–HPNL3 parameter sets lies in the range 671.51 to 596.92 and satisfies the constraint imposed by GW190814 event ($\Lambda_{1.4} = 616^{+273}_{-158}$) [28]. The $\Lambda_{1.4}$ strongly interrelates with $R_{1.4}$. It is noteworthy that the observed $\Lambda_{1.4}$ from the GW170817 event favors the small value of $R_{1.4}$ and hence L too which in turn prefers a somewhat larger value of $\Lambda_{\sigma\delta}$ (HPNL4, HPNL5 models). From this, it can be concluded that if both restrictions on $\Lambda_{1.4}$ from GW170817 and GW190814 are taken into account, then only the HPNL4 and HPNL5 interactions are acceptable as the appropriate EoSs for neutron stars. It is thus possible to mention that $R_{1.4}$ lies around 12.75–12.80 km and L around 52.29–55.44 MeV. In Fig. 11, we display the results of dimensionless tidal deformability $\Lambda_{1.4}$ as a function of mass (M) of neutron stars for various HPNL parametrizations. The value of Λ decreases with an increase in the gravitational mass of the neutron star. It is noteworthy that the value of $\Lambda_{1.4}$ obtained for canonical mass with HPNL4 and HPNL5 parameter sets is 557.14 and 548.01 which satisfies the limit $\Lambda_{1.4} \leqslant 580$ [6]. The Λ calculated for HPNL to HPNL3 parametrizations is also consistent with the findings from [11,72] and satisfies the $\Lambda_{1.4} = 616^{+273}_{-158}$

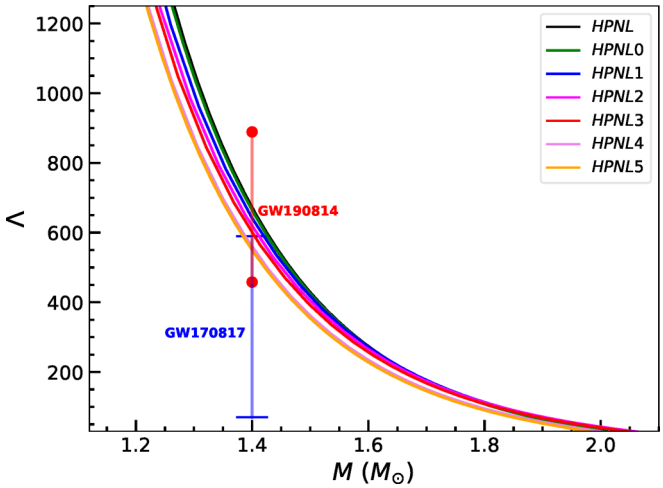

FIG. 11. Variation of dimensionless tidal deformability (Λ) with respect to gravitational mass of neutron star for various HPNL parametrizations.

from GW190814 [28] for the EoS of dense nuclear matter. It can be observed from the figure that the inclusion of mixed interactions $\Lambda_{\sigma\delta}$ in the Lagrangian of the RMF model has a significant effect on tidal deformability Λ.

In Table IV, we summarize the results for nonrotating neutron star properties such as maximum gravitational mass ($M_{\rm max}$), neutron star radius corresponding to the maximum mass ($R_{\rm max}$), radius $R_{1.4}$, central density $\rho_{1.4}$, and tidal deformability ($\Lambda_{1.4}$) corresponding to canonical mass of neutron star.

IV. SUMMARY

Using the RMF model which includes the isoscalar and isovector-scalar mesons mixed interaction ($\Lambda_{\sigma\delta}$) of σ^2-δ^2, in addition to different nonlinear, self-couplings and vector meson mixing of ω^2-ρ^2, the properties of finite nuclei, bulk nuclear matter, and neutron stars are investigated which can sustain the available experimental data both from terrestrial experiments and astrophysical observations of a neutron star. Seven relativistic interactions HPNL, HPNL0, HPNL1, HPNL2, HPNL3, HPNL4, and HPNL5 have been generated for the Lagrangian density given by Eq. (1) to investigate the effect of isoscalar and isovector scalar meson mixed interactions, $\Lambda_{\sigma\delta}$, on the properties of finite nuclei and neutron star matter. The HPNL0, HPNL1, HPNL2, HPNL3, HPNL4, and HPNL5 parametrizations correspond to different values of the isoscalar and isovector scalar meson mixed couplings ($\Lambda_{\sigma\delta}$) of σ-δ mesons, i.e., $\Lambda_{\sigma\delta} = 0.00, 0.01, 0.02, 0.03, 0.04$, and 0.05, respectively. For the sake of comparison, we have also constructed the HPNL parameter set that does not include the coupling (g_δ) of δ meson to the nucleon and couplings ($\Lambda_{\sigma\delta}$) of σ-δ mesons. The isoscalar and isovector scalar meson mixed interactions $\sigma^2\delta^2$ have a significant influence on the density dependence of symmetry energy and neutron star properties. The HPNL interactions successfully account for the binding energies and charge rms radii of several closed/open-shell nuclei. The thick neutron skin thickness (Δr_{np}) observed from PREX-II results is achieved with a somewhat smaller value of L using larger σ-δ meson mixed interaction $\Lambda_{\sigma\delta}$. The density dependence of symmetry energy becomes softer in the low to medium density regime by using larger coupling $\Lambda_{\sigma\delta}$. The σ-δ mixing is found to have a large influence on the radius and tidal deformability of a neutron star. These new RMF models are found to be simultaneously compatible with the constraints on the equation of state of symmetric nuclear and pure neutron matter from particle flow data in heavy ion collisions, the neutron skin thickness of ^{208}Pb from PREX-II results [14], the mass-radius relations measured from NICER [3,4], and the limits of dimensionless tidal deformability of a canonical neutron star from binary neutron star merger GW170817 [6] and GW190814 events [28]. The value of neutron skin thickness (Δr_{np}) for ^{48}Ca nucleus predicted for HPNL parametrizations overestimates the CREX results reported in Ref. [14]. So, it puts serious tension to fit CREX and PREX-II results simultaneously without compromising the properties of finite nuclei, bulk nuclear, and dense matter. In Refs. [11,16,19,20,31,57,73] it is reported that the CREX result pushes the density dependence of symmetry energy (L) towards a lower value, while PREX-II results shifts it towards a higher value and shows the tension to understand the CREX and PREX-II results simultaneously within relativistic mean field models. We are hoping that novel experimental studies are necessary to resolve this tension or discrepancies.

ACKNOWLEDGMENTS

The authors are thankful to Himachal Pradesh University for providing computational facilities. S.K. is highly thankful to CSIR-UGC (Govt. of India) for providing financial assistance (NTA/211610029883) under Junior/Senior Research Fellowship scheme.

[1] P. B. Demorest, Tim Pennucci, S. M. Ransom, M. S. E. Roberts, and J. W. T. Hessels, A two-solar-mass neutron star measured using shapiro delay, Nature (London) **467**, 1081 (2010).

[2] Z. Arzoumanian, A. Brazier, S. Burke-Spolaor, S. Chamberlin, S. Chatterjee, B. Christy, J. M. Cordes, N. J. Cornish, F. Crawford, H. T. Cromartie *et al.*, The nanograv 11-year data set: High-precision timing of 45 millisecond pulsars, Astrophys. J. Suppl. S. **235**, 37 (2018).

[3] M. C. Miller, F. K. Lamb, A. J. Dittmann, S. Bogdanov, Z. Arzoumanian, K. C. Gendreau, S. Guillot, W. C. G. Ho, J. M. Lattimer, M. Loewenstein, S. M. Morsink, P. S. Ray, M. T. Wolff, C. L. Baker, T. Cazeau, S. Manthripragada, C. B. Markwardt, T. Okajima, S. Pollard, I. Cognard, H. T. Cromartie, E. Fonseca, L. Guillemot, M. Kerr, A. Parthasarathy, T. T. Pennucci, S. Ransom, and I. Stairs, The radius of PSR J0740+6620 from NICER and XMM-newton data, Astrophys. J. Lett. **918**, L28 (2021).

[4] T. E. Riley, A. L. Watts, P. S. Ray, S. Bogdanov, S. Guillot, S. M. Morsink, A. V. Bilous, Z. Arzoumanian, D. Choudhury, J. S. Deneva *et al.*, A nicer view of the massive pulsar PSR J0740+ 6620 informed by radio timing and XMM-Newton spectroscopy, Astrophys. J. Lett. **918**, L27 (2021).

[5] B. P. Abbott, R. Abbott, T. D. Abbott, F. Acernese, K. Ackley, C. Adams, T. Adams, P. Addesso, R. X. Adhikari, V. B. Adya *et al.*, GW170817: Observation of gravitational waves from a binary neutron star inspiral, Phys. Rev. Lett. **119**, 161101 (2017).

[6] B. P. Abbott, R. Abbott, T. D. Abbott, F. Acernese, K. Ackley, C. Adams, T. Adams, P. Addesso, R. X. Adhikari, V. B. Adya *et al.*, GW170817: Measurements of neutron star radii and equation of state, Phys. Rev. Lett. **121**, 161101 (2018).

[7] B. P. Abbott, R. Abbott, T. D. Abbott, F. Acernese, K. Ackley, C. Adams, T. Adams, P. Addesso, R. X. Adhikari, V. B. Adya *et al.*, Properties of the binary neutron star merger GW170817, Phys. Rev. X **9**, 011001 (2019).

[8] T. Hinderer, Tidal love numbers of neutron stars, Astrophys. J. **677**, 1216 (2008).

[9] T. Hinderer, B. D. Lackey, R. N. Lang, and J. S. Read, Tidal deformability of neutron stars with realistic equations of state and their gravitational wave signatures in binary inspiral, Phys. Rev. D **81**, 123016 (2010).

[10] D. Adhikari, H. Albataineh, D. Androic, K. Aniol, D. S. Armstrong, T. Averett, C. A. Gayoso, S. Barcus, V. Bellini, R. S. Beminiwattha *et al.*, Accurate determination of the neutron skin thickness of ^{208}Pb through parity-violation in electron scattering, Phys. Rev. Lett. **126**, 172502 (2021).

[11] B. T. Reed, F. J. Fattoyev, C. J. Horowitz, and Jorge Piekarewicz, Implications of PREX-2 on the equation of state of neutron-rich matter, Phys. Rev. Lett. **126**, 172503 (2021).

[12] H. T. Cromartie, E. Fonseca, S. M. Ransom, P. B. Demorest, Z. Arzoumanian, H. Blumer, P. R. Brook, M. E. DeCesar, T. Dolch, J. A. Ellis, R. D. Ferdman, E. C. Ferrara, N. Garver-Daniels, P. A. Gentile, M. L. Jones, M. T. Lam, D. R. Lorimer, R. S. Lynch, M. A. McLaughlin, C. Ng *et al.*, Relativistic Shapiro delay measurements of an extremely massive millisecond pulsar, Nat. Astron. **4**, 72 (2020).

[13] P. Danielewicz, R. Lacey, and W. G. Lynch, Determination of the equation of state of dense matter, Science **298**, 1592 (2002).

[14] D. Adhikari, H. Albataineh, D. Androic, K. A. Aniol, D. S. Armstrong, T. Averett, C. Ayerbe Gayoso, S. K. Barcus, V. Bellini, R. S. Beminiwattha, J. F. Benesch, H. Bhatt, D. Bhatta Pathak, D. Bhetuwal, B. Blaikie, J. Boyd, Q. Campagna, A. Camsonne, G. D. Cates, Y. Chen *et al.*, Precision determination of the neutral weak form factor of ^{48}Ca, Phys. Rev. Lett. **129**, 042501 (2022).

[15] P.-G. Reinhard, X. Roca-Maza, and W. Nazarewicz, Information content of the parity-violating asymmetry in ^{208}Pb, Phys. Rev. Lett. **127**, 232501 (2021).

[16] P.-G. Reinhard, X. Roca-Maza, and W. Nazarewicz, Combined theoretical analysis of the parity-violating asymmetry for ^{48}Ca and ^{208}Pb, Phys. Rev. Lett. **129**, 232501 (2022).

[17] C. Drischler, R. J. Furnstahl, J. A. Melendez, and D. R. Phillips, How well do we know the neutron-matter equation of state at the densities inside neutron stars? A Bayesian approach with correlated uncertainties, Phys. Rev. Lett. **125**, 202702 (2020).

[18] J. Xu, W.-J. Xie, and B.-A. Li, Bayesian inference of nuclear symmetry energy from measured and imagined neutron skin thickness in ^{116,118,120,122,124,130,132}Sn, ^{208}Pb, and ^{48}Ca, Phys. Rev. C **102**, 044316 (2020).

[19] V. Thakur, R. Kumar, P. Kumar, M. Kumar, C. Mondal, K. Huang, J. Hu, B. K. Agrawal, and S. K. Dhiman, Relativistic approach for the determination of nuclear and neutron star properties in consideration of PREX-II results, Phys. Rev. C **107**, 015803 (2023).

[20] M. Kumar, S. Kumar, V. Thakur, R. Kumar, B. K. Agrawal, and S. K. Dhiman, CREX- and PREX-II-motivated relativistic interactions and their implications for the bulk properties of nuclear matter and neutron stars, Phys. Rev. C **107**, 055801 (2023).

[21] R. Kumar, B. K. Agrawal, and S. K. Dhiman, Effects of ω meson self-coupling on the properties of finite nuclei and neutron stars, Phys. Rev. C **74**, 034323 (2006).

[22] J. Estee, W. G. Lynch, C. Y. Tsang, J. Barney, G. Jhang, M. B. Tsang, R. Wang, M. Kaneko, J. W. Lee, T. Isobe, M. Kurata-Nishimura, T. Murakami, D. S. Ahn, L. Atar, T. Aumann, H. Baba, K. Boretzky, J. Brzychczyk, G. Cerizza, N. Chiga *et al.*, Probing the symmetry energy with the spectral pion ratio, Phys. Rev. Lett. **126**, 162701 (2021).

[23] J. Piekarewicz, Implications of PREX-2 on the electric dipole polarizability of neutron-rich nuclei, Phys. Rev. C **104**, 024329 (2021).

[24] V. Thakur, R. Kumar, P. Kumar, V. Kumar, B. K. Agrawal, and S. K. Dhiman, Relativistic mean field model parametrizations in the light of GW170817, GW190814, and PSR J 0740+ 6620, Phys. Rev. C **106**, 025803 (2022).

[25] V. Thakur, R. Kumar, P. Kumar, V. Kumar, M. Kumar, C. Mondal, B. K. Agrawal, and S. K. Dhiman, Effects of an isovector scalar meson on the equation of state of dense matter within a relativistic mean field model, Phys. Rev. C **106**, 045806 (2022).

[26] R. Kumar, M. Kumar, V. Thakur, S. Kumar, P. Kumar, A. Sharma, B. K. Agrawal, and S. K. Dhiman, Observational constraint from the heaviest pulsar PSR J0952-0607 on the equation of state of dense matter in relativistic mean field model, Phys. Rev. C **107**, 055805 (2023).

[27] R. J. Furnstahl, B. D. Serot, and H.-B. Tang, A chiral effective Lagrangian for nuclei, Nucl. Phys. A **615**, 441 (1997).

[28] R. Abbott *et al.*, GW190814: Gravitational waves from the coalescence of a 23 solar mass black hole with a 2.6 solar mass compact object, Astrophys. J. Lett. **896**, L44 (2020).

[29] S. K. Dhiman, R. Kumar, and B. K. Agrawal, Nonrotating and rotating neutron stars in the extended field theoretical model, Phys. Rev. C **76**, 045801 (2007).

[30] N. K. Glendenning, *Compact Stars: Nuclear Physics, Particle Physics, and General Relativity* (Springer-Verlag, New York, 2000).

[31] T. Miyatsu, M.-K. Cheoun, K. Kim, and K. Saito, Can the PREX-2 and CREX results be understood by relativistic mean-field models with the astrophysical constraints?, Phys. Lett. B **843**, 138013 (2023).

[32] F. Li, B.-J. Cai, Y. Zhou, W.-Z. Jiang, and L.-W. Chen, Effects of isoscalar- and isovector-scalar meson mixing on neutron star structure, Astrophys. J. **929**, 183 (2022).

[33] T. J. Bürvenich, D. G. Madland, and P.-G. Reinhard, Adjustment studies in self-consistent relativistic mean-field models, Nucl. Phys. A **744**, 92 (2004).

[34] S. Kirkpatrick, Optimization by simulated annealing: Quantitative studies, J. Stat. Phys. **34**, 975 (1984).
[35] J. Dobaczewski, W. Nazarewicz, and P. G. Reinhard, Error estimates of theoretical models: A guide, J. Phys. G: Nucl. Part. Phys. **41**, 074001 (2014).
[36] M. Wang, W. J. Huang, F. G. Kondev, G. Audi, and S. Naimi, The AME 2020 atomic mass evaluation (II). Tables, graphs and references*, Chin. Phys. C **45**, 030003 (2021).
[37] I. Angeli and K. P. Marinova, Table of experimental nuclear ground state charge radii: An update, At. Data Nucl. Data Tables **99**, 69 (2013).
[38] P. Ring and P. Schuck, *The Nuclear Many-Body Problem* (Springer Science & Business Media, New York, 1980).
[39] S. Karatzikos, A. V. Afanasjev, G. A. Lalazissis, and P. Ring, The fission barriers in actinides and superheavy nuclei in covariant density functional theory, Phys. Lett. B **689**, 72 (2010).
[40] T. Duguet, P. Bonche, P.-H. Heenen, and J. Meyer, Pairing correlations. II. Microscopic analysis of odd-even mass staggering in nuclei, Phys. Rev. C **65**, 014311 (2001).
[41] E. Fonseca, H. T. Cromartie, T. T. Pennucci, P. S. Ray, A. Yu. Kirichenko, S. M. Ransom, P. B. Demorest, I. H. Stairs, Z. Arzoumanian, L. Guillemot *et al.*, Refined mass and geometric measurements of the high-mass PSR J0740+ 6620, Astrophys. J. Lett. **915**, L12 (2021).
[42] H. Mueller and B. D. Serot, Relativistic mean-field theory and the high-density nuclear equation of state, Nucl. Phys. A **606**, 508 (1996).
[43] B. K. Pradhan, D. Chatterjee, R. Gandhi, and J. Schaffner-Bielich, Role of vector self-interaction in neutron star properties, Nucl. Phys. A **1030**, 122578 (2022).
[44] S. Malbrunot-Ettenauer, S. Kaufmann, S. Bacca, C. Barbieri, J. Billowes, M. L. Bissell, K. Blaum, B. Cheal, T. Duguet, R. F. Garcia Ruiz, W. Gins, C. Gorges, G. Hagen, H. Heylen, J. D. Holt, G. R. Jansen, A. Kanellakopoulos, M. Kortelainen, T. Miyagi, P. Navrátil, W. Nazarewicz *et al.*, Nuclear charge radii of the nickel isotopes $^{58-68,70}$Ni, Phys. Rev. Lett. **128**, 022502 (2022).
[45] W. G. Lynch, M. B. Tsang, Y. Zhang, P. Danielewicz, M. Famiano, Z. Li, and A. W. Steiner, Probing the symmetry energy with heavy ions, Prog. Part. Nucl. Phys. **62**, 427 (2009).
[46] T.-G. Yue, L.-W. Chen, Z. Zhang, and Y. Zhou, Constraints on the symmetry energy from PREX-II in the multimessenger era, Phys. Rev. Res. **4**, L022054 (2022).
[47] B.-A. Li, B.-J. Cai, W.-J. Xie, and N.-B. Zhang, Progress in constraining nuclear symmetry energy using neutron star observables since GW170817, Universe **7**, 182 (2021).
[48] W.-C. Chen and J. Piekarewicz, Searching for isovector signatures in the neutron-rich oxygen and calcium isotopes, Phys. Lett. B **748**, 284 (2015).
[49] M. Wang, G. Audi, F. G. Kondev, W. J. Huang, S. Naimi, and Xing Xu, The AME2016 atomic mass evaluation, Chin. Phys. C **41**, 030003 (2017).
[50] J. Birkhan, M. Miorelli, S. Bacca, S. Bassauer, C. A. Bertulani, G. Hagen, H. Matsubara, P. von Neumann-Cosel, T. Papenbrock, N. Pietralla, V. Yu. Ponomarev, A. Richter, A. Schwenk, and A. Tamii, Electric dipole polarizability of ^{48}Ca and implications for the neutron skin, Phys. Rev. Lett. **118**, 252501 (2017).
[51] L.-W. Chen, B.-J. Cai, C. M. Ko, B.-A. Li, C. Shen, and J. Xu, Higher-order effects on the incompressibility of isospin asymmetric nuclear matter, Phys. Rev. C **80**, 014322 (2009).
[52] H. Sotani and S. Ota, Neutron star mass formula with nuclear saturation parameters for asymmetric nuclear matter, Phys. Rev. D **106**, 103005 (2022).
[53] J. M. Lattimer, Constraints on nuclear symmetry energy parameters, Particles **6**, 30 (2023).
[54] G. Colo, U. Garg, and H. Sagawa, Symmetry energy from the nuclear collective motion: Constraints from dipole, quadrupole, monopole and spin-dipole resonances, Eur. Phys. J. A **50**, 26 (2014).
[55] J. Piekarewicz, Symmetry energy constraints from giant resonances: A relativistic mean-field theory overview, Eur. Phys. J. A **50**, 25 (2014).
[56] B.-A. Li and X. Han, Constraining the neutron–proton effective mass splitting using empirical constraints on the density dependence of nuclear symmetry energy around normal density, Phys. Lett. B **727**, 276 (2013).
[57] Z. Zhang and L.-W. Chen, Bayesian inference of the symmetry energy and the neutron skin in ^{48}Ca and ^{208}Pb from CREX and PREX-2, arXiv:2207.03328.
[58] J. Zimmerman, Z. Carson, K. Schumacher, A. W. Steiner, and K. Yagi, Measuring nuclear matter parameters with nicer and Ligo/Virgo, arXiv:2002.03210.
[59] T. Li, U. Garg, Y. Liu, R. Marks, B. K. Nayak, P. V. Madhusudhana Rao, M. Fujiwara, H. Hashimoto, K. Nakanishi, S. Okumura, M. Yosoi, M. Ichikawa, M. Itoh, R. Matsuo, T. Terazono, M. Uchida, Y. Iwao, T. Kawabata, T. Murakami, H. Sakaguchi, S. Terashima *et al.*, Isoscalar giant resonances in the Sn nuclei and implications for the asymmetry term in the nuclear-matter incompressibility, Phys. Rev. C **81**, 034309 (2010).
[60] D. Patel, U. Garg, M. Fujiwara, H. Akimune, G. P. A. Berg, M. N. Harakeh, M. Itoh, T. Kawabata, K. Kawase, B. K. Nayak, T. Ohta, H. Ouchi, J. Piekarewicz, M. Uchida, H. P. Yoshida, and M. Yosoi, Giant monopole resonance in even-a Cd isotopes, the asymmetry term in nuclear incompressibility, and the "softness" of Sn and Cd nuclei, Phys. Lett. B **718**, 447 (2012).
[61] M. G. Alford, S. Han, and M. Prakash, Generic conditions for stable hybrid stars, Phys. Rev. D **88**, 083013 (2013).
[62] G. Baym, C. Pethick, and P. Sutherland, The ground state of matter at high densities: Equation of state and stellar models, Astrophys. J. **170**, 299 (1971).
[63] J. R. Oppenheimer and G. M. Volkoff, On massive neutron cores, Phys. Rev. **55**, 374 (1939).
[64] R. C. Tolman, Static solutions of Einstein's field equations for spheres of fluid, Phys. Rev. **55**, 364 (1939).
[65] E. Fonseca, T. T. Pennucci, J. A. Ellis, I. H. Stairs, D. J. Nice, S. M. Ransom, P. B. Demorest, Z. Arzoumanian, K. Crowter, T. Dolch *et al.*, The nanograv nine-year data set: Mass and geometric measurements of binary millisecond pulsars, Astrophys. J. **832**, 167 (2016).
[66] L. Rezzolla, E. R. Most, and L. R. Weih, Using gravitational-wave observations and quasi-universal relations to constrain the maximum mass of neutron stars, Astrophys. J. Lett. **852**, L25 (2018).
[67] T. E. Riley, A. L. Watts, S. Bogdanov, P. S. Ray, R. M. Ludlam, S. Guillot, Z. Arzoumanian, C. L. Baker, A. V. Bilous, D. Chakrabarty, K. C. Gendreau, A. K. Harding, W. C. G. Ho, J. M. Lattimer, S. M. Morsink, and T. E. Strohmayer, A NICER view of PSR J0030+0451: Millisecond pulsar parameter estimation, Astrophys. J. Lett. **887**, L21 (2019).

[68] M. C. Miller, F. K. Lamb, A. J. Dittmann, S. Bogdanov, Z. Arzoumanian, K. C. Gendreau, S. Guillot, A. K. Harding, W. C. G. Ho, J. M. Lattimer, R. M. Ludlam, S. Mahmoodifar, S. M. Morsink, P. S. Ray, T. E. Strohmayer, K. S. Wood, T. Enoto, R. Foster, T. Okajima, G. Prigozhin *et al.*, PSR J0030+0451 mass and radius from NICER data and implications for the properties of neutron star matter, Astrophys. J. Lett. **887**, L24 (2019).

[69] E. Annala, T. Gorda, A. Kurkela, and A. Vuorinen, Gravitational-wave constraints on the neutron-star-matter equation of state, Phys. Rev. Lett. **120**, 172703 (2018).

[70] T. Hinderer, Erratum: Tidal love numbers of neutron stars (2008, APJ, 677, 1216), Astrophys. J. **697**, 964 (2009).

[71] T. Damour and A. Nagar, Effective one body description of tidal effects in inspiralling compact binaries, Phys. Rev. D **81**, 084016 (2010).

[72] Y. Li, H. Chen, D. Wen, and J. Zhang, Constraining the nuclear symmetry energy and properties of the neutron star from GW170817 by Bayesian analysis, Eur. Phys. J. A **57**, 1 (2021).

[73] E. Yüksel and N. Paar, Implications of parity-violating electron scattering experiments on ^{48}Ca (CREX) and ^{208}Pb (PREX-II) for nuclear energy density functionals, Phys. Lett. B **836**, 137622 (2023).